Journal of Pharmaceutical Analysis 9 (2019) 358–366

Contents lists available at ScienceDirect

Journal of Pharmaceutical Analysis

journal homepage: www.elsevier.com/locate/jpa

Original Article

# Highly sensitive simultaneous electrochemical determination of myricetin and rutin via solid phase extraction on a ternary Pt@r-GO@MWCNTs nanocomposite

Satar Tursynbolat, Yrysgul Bakytkarim, Jianzhi Huang, Lishi Wang*

*School of Chemistry and Chemical Engineering, South China University of Technology, Guangzhou 510641, China*

ARTICLE INFO

*Article history:*
Received 15 December 2018
Received in revised form
18 March 2019
Accepted 19 March 2019
Available online 22 March 2019

*Keywords:*
Ternary nanocomposite
Simultaneous determination
Electrochemical sensor
Myricetin
Rutin

ABSTRACT

The simultaneous electrochemical determination of myricetin and rutin remains a challenge due to their indistinguishable potentials. To solve this problem, we constructed a ternary platinum nanoparticle, reduced graphene oxide, multi-walled carbon nanotubes (Pt@r-GO@MWCNTs) nanocomposite via a facile one-pot synthetic method. Under the optimized conditions, the ternary Pt@r-GO@MWCNTs nanocomposite exhibited good electrocatalytic activity toward myricetin and rutin via solid phase extraction and excellent performance for the simultaneous determination of myricetin and rutin. The oxidation peak current of myricetin was proportional to its concentrations in the range of 0.05–50 μM with a detection limit of 0.01 μM (S/N = 3). The linear range for rutin was 0.05–50 μM with a detection limit of 0.005 μM (S/N = 3). The ternary nanocomposite sensor also exhibited good reproducibility and stability, and was successfully used for the simultaneous determination of myricetin and rutin in real orange juice samples with recoveries ranging between 100.57% and 108.46%.



## 1. Introduction

Flavonoids have received significant attention due to their effects on human health. In particular, myricetin and rutin are two important flavonoids naturally present in plants including berries, tea, fruits, vegetables, and medicinal herbs [1]. According to previous reports, myricetin exhibits anti-oxidant, anti-cancer, and cytoprotective properties [2]. Rutin has a wide range of physiological functions, such as anti-inflammatory, anti-bacterial, anti-aging, and anti-oxidation abilities [3]. Because of the above listed pharmacological effects, health foods, drinks, and medicinal herbs usually contain myricetin and rutin. Therefore, it is important to develop a method to determine the contents of myricetin and rutin in food and medicine.

To date, some analytical methods have been developed to simultaneously detect myricetin and rutin, including capillary electrophoresis [4,5], chemiluminescence [6], high performance liquid chromatography (HPLC) [7], and spectrophotometry [8]. These methods can sensitively detect myricetin and rutin, but they have many drawbacks including the need for expensive equipment and time-consuming experimental processes, which constrain their practical application [9–18]. Compared to previously developed methods, voltammetry provides a fast response, uses simple equipment, and is highly sensitive to the determination of myricetin or rutin [19–28]. Although many electrochemical sensors have been reported for single determinations of myricetin or rutin [29–35], their simultaneous determination has seldom been reported due to their analogous chemical structures and electrochemical characteristics, resulting in an indistinguishable potential [36,37]. Therefore, it is imperative to develop an electrochemical sensor that can realize the simultaneous determination of myricetin and rutin.

Multi-walled carbon nanotubes (MWCNTs) and reduced graphene oxide (r-GO) are promising conductor materials with high surface area, stable physical and chemical properties, high mechanical strength, and good absorption properties [38–47]. In addition, they are easily combined with other nanomaterials due to their constituent hydroxyl (−OH), carboxyl (−COOH), and carbonyl (−C═O) functional groups [48–51]. The noble metal Pt is widely used in the field of catalysis and fuel cells [52]. Pt nanoparticles have been loaded into carbon nanotubes to form novel composite materials that show good performances as electrochemical sensors [53–55].

Peer review under responsibility of Xi'an Jiaotong University.
* Corresponding author.
*E-mail address:* wanglsh@scut.edu.cn (L. Wang).

https://doi.org/10.1016/j.jpha.2019.03.009

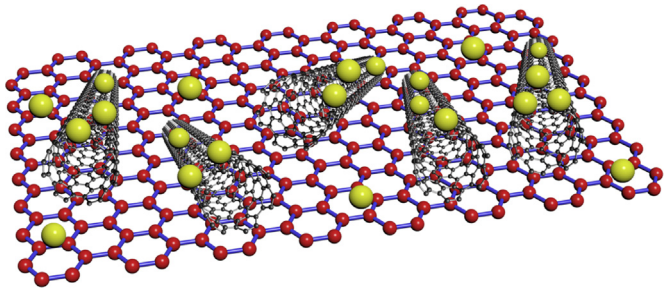

**Scheme 1.** Fabrication of the ternary Pt@r-GO@MWCNTs nanocomposite.

In this study, we synthesized a novel ternary nanocomposite consisting of Pt NPs, MWCNTs and r-GO for the simultaneous determination of myricetin and rutin. The ternary nanocomposite was fabricated by a facile one-pot synthesis method and showed strong ability to adsorb myricetin and rutin during solid-phase extraction. Because of this excellent property, the proposed nanocomposite sensor exhibits a distinguishable potential, high response, wide linear detection range, and low detection limit for both myricetin and rutin. In addition, this sensor exhibits good reproducibility, reversibility, and stability and was successfully used in the quantitative determination of myricetin and rutin in real orange juice samples, yielding satisfactory results.

## 2. Experimental

### 2.1. Chemicals and reagents

Rutin (98%, analytical grade) and chloroplatinic acid ($H_2PtCl_6$) were purchased from J&K Chemical Corporation (Beijing, China). Myricetin (97%, analytical grade) was obtained from Tokyo Chemical Industry (TCI) Co., Ltd. The MWCNTs (95%, analytical grade) were purchased from Aladdin Chemical Reagent Co., Ltd. (Shanghai, China). All other chemicals were of analytical grade. Britton-Robinson (BR) buffer was prepared by mixing acetic acid, phosphoric acid, and boric acid. Various pH values of the 0.04 M BR buffer were obtained by adding 0.2 M NaOH and HCl. Stock solutions of 1.0 mmol/dm$^3$ myricetin and 1.0 mmol/dm$^3$ rutin were obtained by dissolution in 50 mL of ethanol and subsequent dilution with doubly distilled water to 100 mL. All aqueous solutions were prepared with doubly distilled water.

### 2.2. Fabrication of the ternary Pt@r-GO@MWCNTs nanocomposite

A novel one-pot method was used to synthesize the ternary Pt@r-GO@MWCNTs nanocomposites at room conditions (room temperature is 25 °C) (Scheme 1). First, 30 mg of monolayer graphene oxide and 30 mg of MWCNTs were placed in 30 mL of double distilled water and mixed for 30 min under ultrasonication. Subsequently, under stirring conditions, 500 μL of a 60 mM $H_2PtCl_6$ solution was added to the above solution. Simultaneously, 10 mL of a 0.05 g/mL $NaBH_4$ solution was added and the reaction mixture

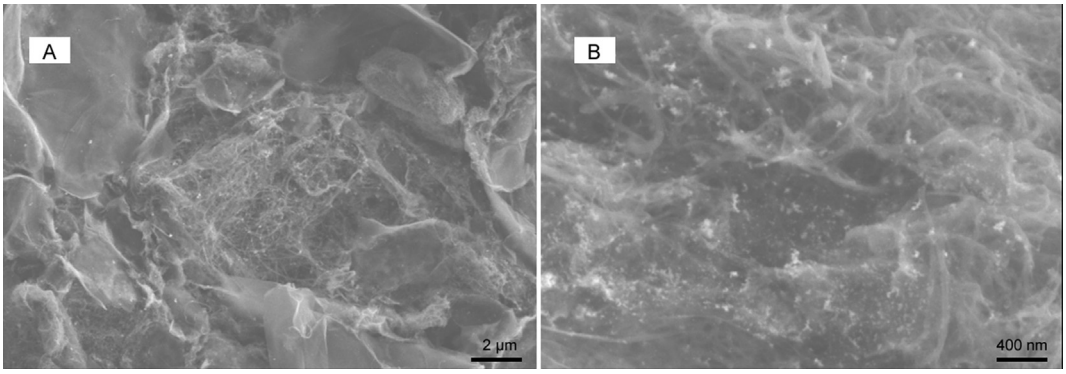


**Fig. 1.** SEM images at (A) low and (B) high magnification of the Pt@r-GO@MWCNTs nanocomposite.

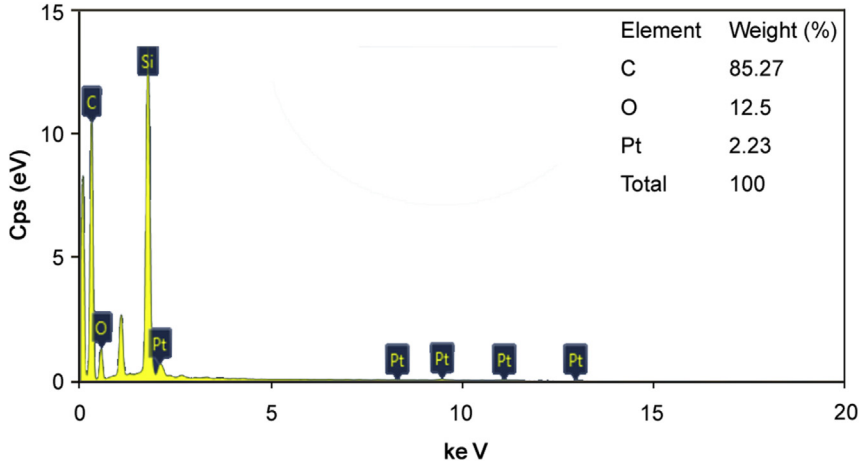


**Fig. 2.** EDS of Pt@r-GO@MWCNTs. Inset is the elemental contents.

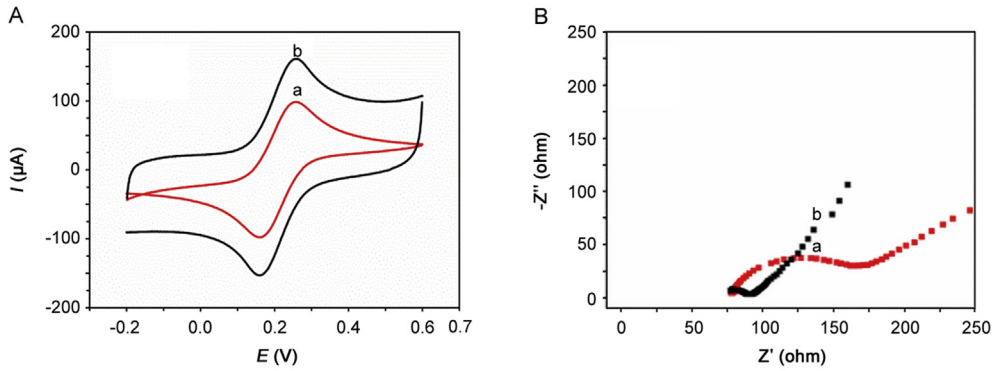


**Fig. 3.** (A) CVs and (B) EIS of the bare GCE (a) and Pt@r-GO@MWCNTs/GCE (b) in 5.0 mmol/dm$^3$ $K_3[Fe(CN)_6]/K_4[Fe(CN)_6]$ containing 0.1 M KCl.

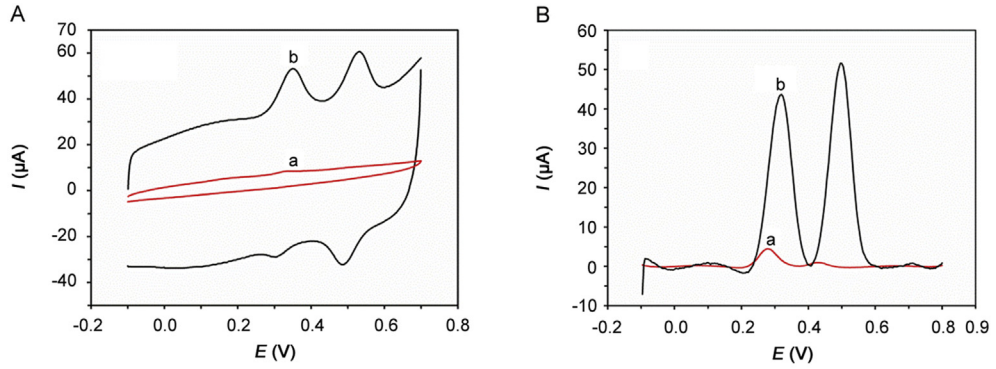


**Fig. 4.** (A) CVs and (B) DPVs of 50 μM myricetin and 50 μM rutin using the bare GCE (a) and Pt@r-GO@MWCNTs/GCE (b) in pH 3.0 BR buffer solutions.

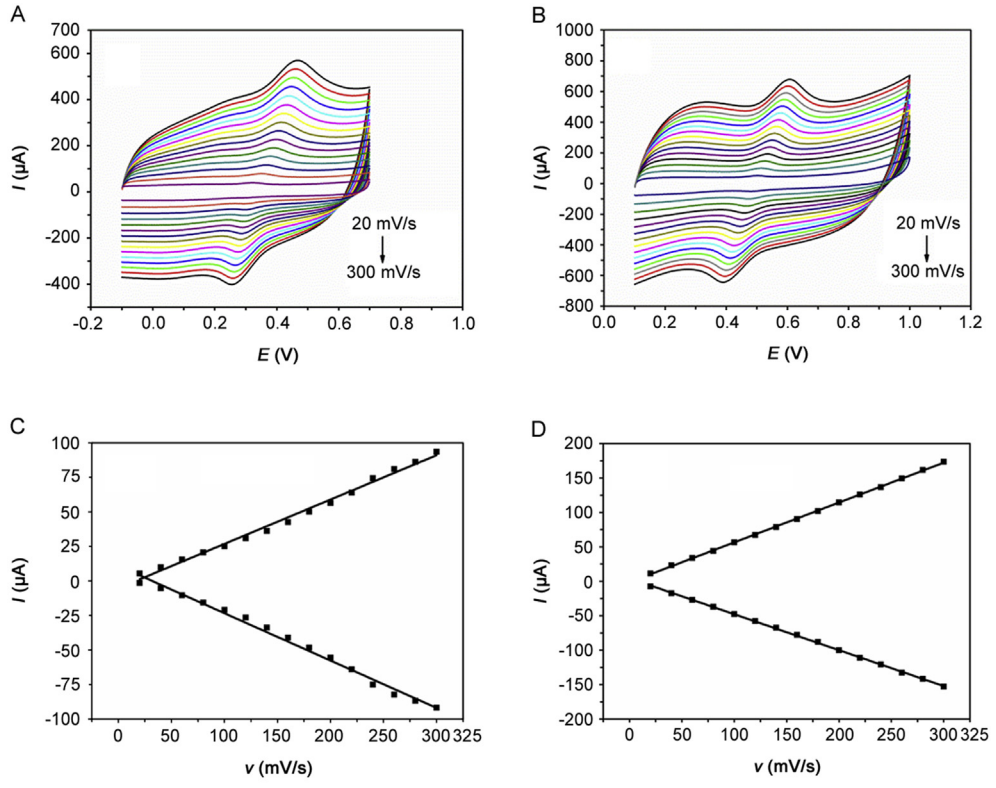


**Fig. 5.** CVs of the Pt@r-GO@MWCNTs/GCE in pH 3.0 BR buffer solution containing (A) 50 μM myricetin and (B) 50 μM rutin at different scan rates (20–300 mV/s). The relationships of oxidation and reduction peak currents of (C) myricetin and (D) rutin with scan rates are also provided.

was stirred vigorously for 30 min. The product was washed three times with a mixed solution of ethanol and water at a ratio of 1:1. Finally, 8 mL of an ethanol and water mixture at a ratio of 1:3 was added to the product, yielding the ternary Pt@r-GO@MWCNTs nanocomposite.

### 2.3. Fabrication of the ternary Pt@r-GO@MWCNTs nanocomposite sensor

First, a glassy carbon electrode (GCE, 3 mm in diameter) was polished with 0.3 and 0.05 μm alumina powders, then rinsed ultrasonically with absolute alcohol and distilled water, and dried under a nitrogen stream. Subsequently, 5 μL of a homogeneous suspension of Pt@r-GO@MWCNTs was dropped onto the electrode surface and dried at room temperature (room temperature is 25 °C) to obtain the Pt@r-GO@MWCNTs nanocomposite sensor.

### 2.4. Instrumentation and methods

Electrochemical cyclic voltammetry (CV), electrochemical impedance spectroscopy (EIS), and differential pules voltammetry (DPV) measurements were performed using a CHI 660B electrochemical workstation (Chenhua Co. Ltd. Shanghai, China). A three-electrode system consisting of a bare or modified GCE (3 mm in diameter) working electrode, platinum wire counter electrode, and saturated calomel reference electrode (SCE) was used. DPV scans from −0.1–0.8 V with an amplitude of 0.05 V, pulse width of 0.05 s, pulse period of 0.5 s, and increment of 0.004 V were performed. For CV, scan rate was 50 mV/s and sample interval was 0.001 V. EIS was obtained in a 5.0 mmol/dm$^3$ $K_3[Fe(CN)_6]/K_4[Fe(CN)_6]$ solution containing 0.1 M KCl under an open circuit potential at a frequency range from 0.1 Hz to 100 kHz and 5 mV amplitude. The surface morphology was characterized via field emission scanning electron microscopy (FE-SEM; Zeiss Ultra 55, Germany) and energy dispersive X-ray spectroscopy (EDS).

## 3. Results and discussion

### 3.1. Morphology and characterization of the nanocomposite

Fig. 1 shows the SEM images at low and high magnifications of the ternary Pt@r-GO@MWCNTs nanocomposites. The MWCNTs and r-GO were clearly observed, and the Pt NPs were uniformly and densely distributed in the MWCNTs and r-GO. The Pt@r-GO@MWCNTs composite was also analyzed by EDS (Fig. 2), showing that the main components were C, O and Pt at approximately 85.27, 12.5, and 2.23 wt%, respectively (Si was also observed because the Pt@r-GO@MWCNTs nanocomposite was dropped onto the silicon wafer for SEM sample preparation). The above results indicate the successful fabrication of the Pt@r-GO@MWCNTs nanocomposite.

### 3.2. Electrochemical characterization of the Pt@r-GO@MWCNTs/GCE modified electrode

CV and EIS were performed for the electrochemical characterization of the Pt@r-GO@MWCNTs/GCE electrode. Fig. 3A shows the CVs of different electrodes in a 5.0 mmol/dm$^3$ $K_3[Fe(CN)_6]/K_4[Fe(CN)_6]$ solution containing 0.1 M KCl at 50 mV/s. A pair of reversible redox peaks were observed at +0.26 and + 0.17 V for the bare GCE (curve a). After modification with the Pt@r-GO@MWCNTs nanocomposite (curve b), the redox peak currents increased and a larger background current was observed due to the Pt@r-GO@MWCNTs nanocomposite dramatically increasing the electrode surface area and exhibiting good electrical conductivity [41,42]. Fig. 3B shows the EIS plots of the bare GCE and Pt@r-GO@MWCNTs/GCE. The bare GCE (curve a) exhibited a small resistance, but when the Pt@r-GO@MWCNTs nanocomposite GCE was used (curve b), it displayed a significantly smaller resistance. Therefore, the CV and EIS diagrams further demonstrate the successful preparation of the Pt@r-GO@MWCNTs/GCE sensor.

### 3.3. Electrochemical behavior of myricetin and rutin

The CVs of bare GCE and Pt@r-GO@MWCNTs/GCE in 50 μM myricetin and 50 μM rutin solutions are shown in Fig. 4A. Unlike the bare GCE, two pairs of redox peaks of myricetin and rutin were clearly observed when the Pt@r-GO@MWCNTs/GCE was used along with a larger background current. Thus, the Pt@r-GO@MWCNTs nanocomposite showed a good electrocatalytic effect for detection of both myricetin and rutin. In addition, the DPV results shown in Fig. 4B for the bare GCE ($I_{pa}$ = 4.617 μA, $E_{pa}$ = 0.276 V for myricetin, and $I_{pa}$ = 1.316 μA, $E_{pa}$ = 0.432 V for rutin) provided very small current signals. Moreover, the potential differences were insufficient to realize the simultaneous determination of myricetin

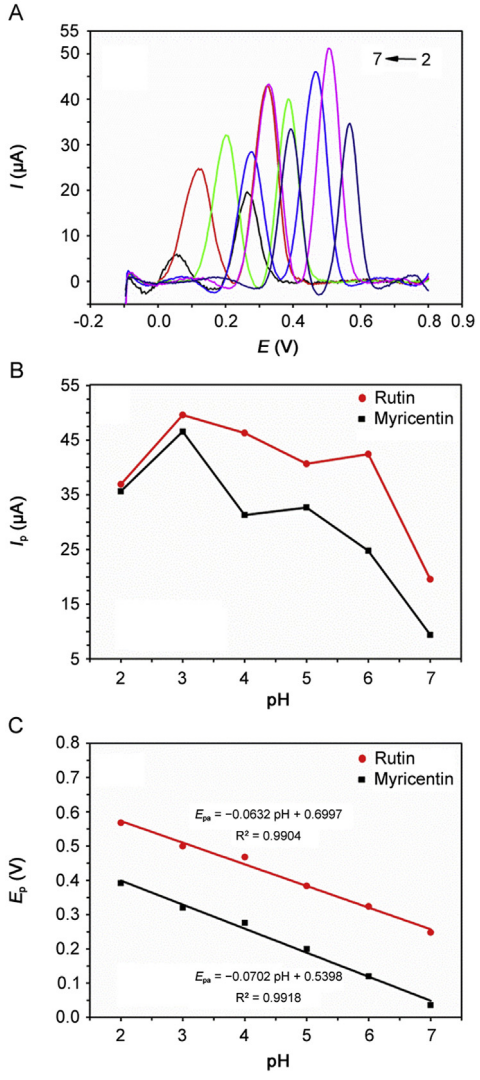


**Fig. 6.** (A) DPVs of 50 μM myricetin and rutin in BR buffer at different pH values on the Pt@r-GO@MWCNTs/GCE nanocomposite sensor. (B) The relationship between pH and oxidation peak currents of myricetin and rutin. (C) The relationship between pH and oxidation peak potentials of myricetin and rutin.

and rutin. However, after modification of the GCE with the Pt@r-GO@MWCNTs nanocomposite (curve b, $I_{pa} = 44.45$ μA, $E_{pa} = 0.320$ V for myricetin, and $I_{pa} = 51.71$ μA, $E_{pa} = 0.496$ V for rutin), the oxidation peak current signals increased by a factors of 11 and 50 for myricetin and rutin, respectively, over that of the bare GCE. In addition, the potential differences became large enough for the simultaneous detection of myricetin and rutin. Therefore, the Pt@r-GO@MWCNTs/GCE sensor was successful used for the simultaneous determination of myricetin and rutin.

### 3.4. Effect of scan rate

The effects of scan rate were investigated by CVs in a pH 3.0 BR buffer solution containing 50 μM myricetin and rutin. As shown in Figs. 5A and B, with an increase in scan rate, both redox currents increased linearly. Figs. 5C and D show the linear equations for myricetin, $I_{pa}$ (μA) = 0.3211ν (mV/s) – 5.2034 ($R^2 = 0.9912$) and $I_{pc}$ (μA) = −0.3428ν (mV/s) + 10.9990 ($R^2 = 0.9902$), and for rutin $I_{pa}$ (μA) = 0.5782ν (mV/s) – 1.3055 ($R^2 = 0.9997$) and $I_{pc}$ (μA) = 0.5214ν (mV/s) + 4.3750 ($R^2 = 0.9996$). These results indicate that the electrocatalytic reactions of both myricetin and rutin on the Pt@r-GO@MWCNTs/GCE are typical adsorption-controlled processes.

### 3.5. The effect of pH

The effect of pH was investigated by DPVs in BR buffer solution containing 50 μM myricetin and rutin at different pH values (Fig. 6A). As the pH increased (Fig. 6B), oxidation peak currents of both myricetin and rutin increased until pH 3 and then decreased at higher pH values. Therefore, the optimum pH was determined to be 3. In Fig. 6C, as the pH increased, both oxidation peak potentials of myricetin and rutin negatively shifted with a good linear relationship between the oxidation peak potentials and pH. The linear equation for myricetin was $E_{pa}$ (V) = −0.0702 pH + 0.5398 ($R^2 = 0.9918$) and for rutin $E_{pa}$ (V) = −0.0632 pH + 0.6997 ($R^2 = 0.9904$). The slopes of the respective equations were 70.2 and 63.2 mV/pH, suggesting that both myricetin and rutin oxidation followed the Nernst equation requiring identical number of protons and electrons. Combined with previous reports [36,37], the myricetin and rutin oxidation mechanism involved the same number electron and proton transfer processes (Scheme 2).

### 3.6. The effects of pre-concentration time and pre-concentration potential

The pre-concentration time and potential were studied in the pH 3 BR buffer solution containing 50 μM myricetin and rutin. In Fig. 7A, at the pre-concentration potential of −0.3 V, the oxidation peak current increased progressively with an increase in pre-concentration time and achieved a maximum value when the pre-concentration time was 550 s, and decreased afterwards. Therefore, the pre-concentration time of 550 s was applied in subsequent studies. Moreover, we studied the effect of pre-

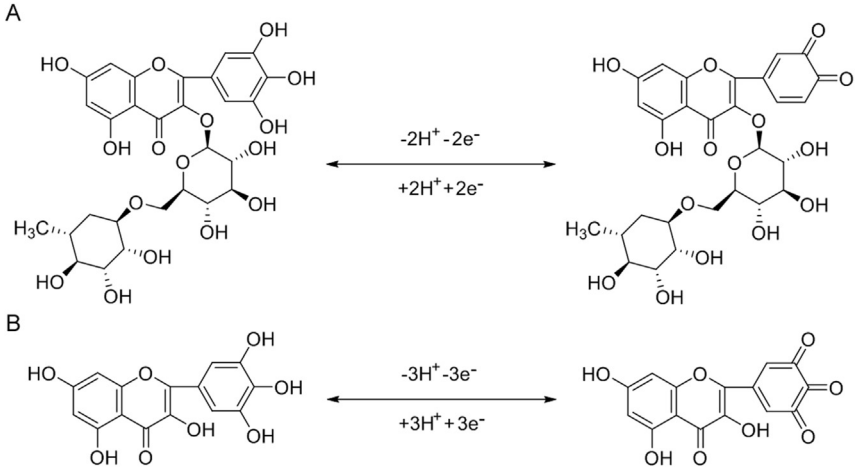


**Scheme 2.** The reaction mechanisms of (A) myricetin and (B) rutin.

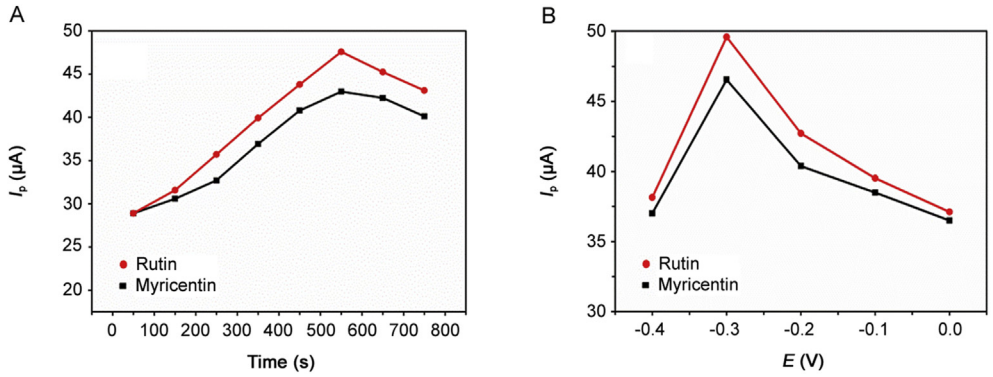


**Fig. 7.** Effect of (A) pre-concentration time and (B) pre-concentration potential on the oxidation peak currents of 50.0 μM myricetin and 50.0 μM rutin at the Pt@r-GO@MWCNTs/GCE in pH 3.0 BR buffer solution.

concentration potential on the oxidation peak currents of myricetin and rutin using the optimized pre-concentration time. In Fig. 7B, the oxidation peak current increased until −0.3 V, after which the oxidation peak currents gradually decreased. Therefore, the optimal pre-concentration potential for determination of myricetin and rutin was −0.3 V.

### 3.7. Quantitative determination of myricetin and rutin

Fig. 8A shows the individual quantitative determination of different concentrations of myricetin in the presence of 2 μM rutin in the pH 3 BR buffer solution. Fig. 8B shows two linear detection ranges of 0.05–10 and 10–50 μM between the oxidation peak

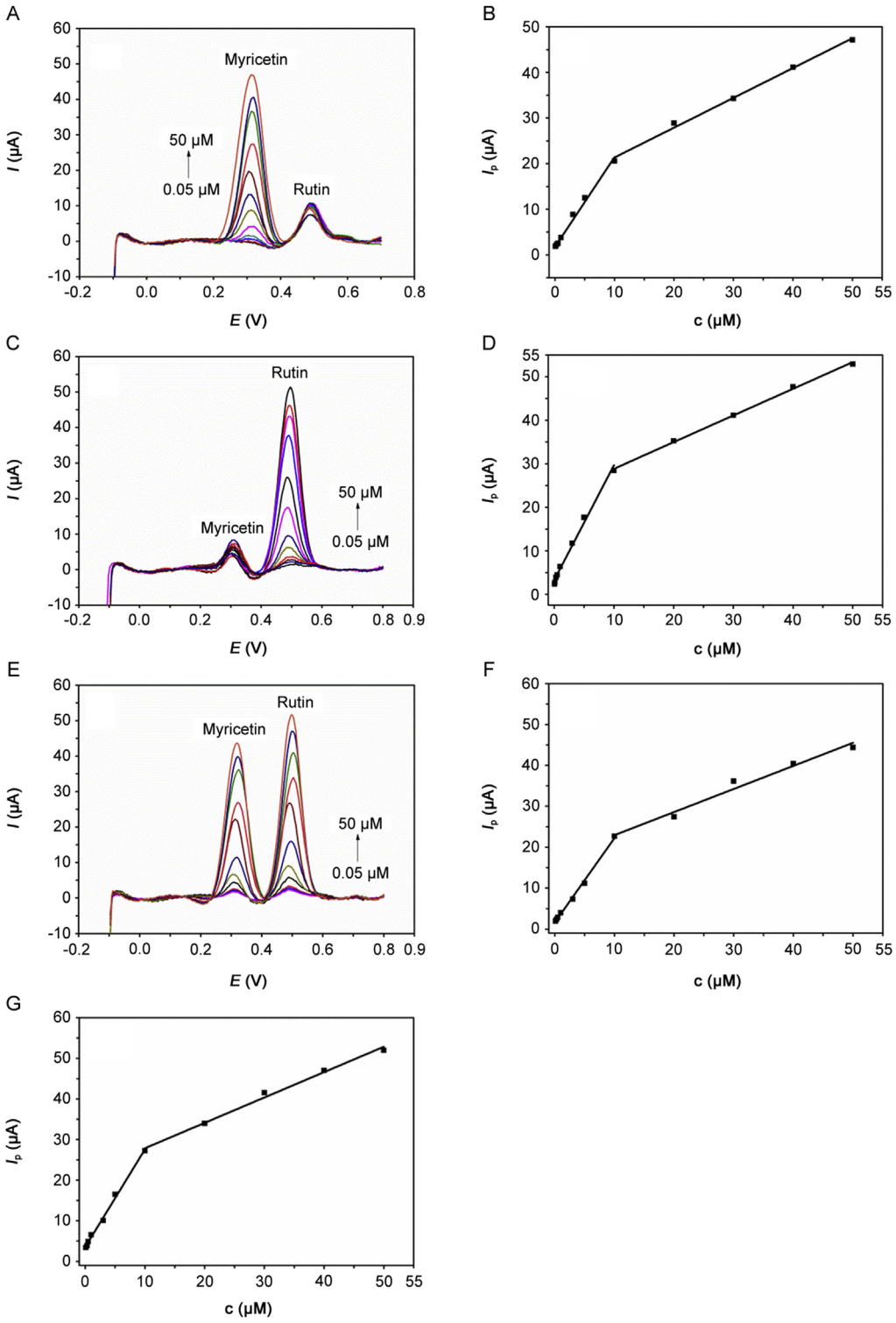


**Fig. 8.** (A) DPVs of myricetin at different concentrations (0.05–50 μM) in BR buffer (pH = 3) in the presence of 2 μM rutin at the Pt@r-GO@MWCNTs/GCE. (B) Linear relationship between the oxidation peak current and concentration of myricetin. (C) DPVs of rutin at different concentrations (0.05–50 μM) in BR buffer (pH = 3) in the presence of 2 μM myricetin at the Pt@r-GO@MWCNTs/GCE. (D) Linear relationship between oxidation peak current and concentration of rutin. (E) DPVs of myricetin and rutin at different concentrations (0.05–50 μM) in BR buffer (pH = 3) at the Pt@r-GO@MWCNTs/GCE. The linear relationships between oxidation peak currents and concentration of (F) myricetin and (G) rutin.

**Table 1**
Comparison of detection performances of the developed sensor and other electrochemical devices reported for detection of myricetin or rutin.

| Electrode | Method | Linear range (μM) | Limit of detection (nM) | Reference |
|---|---|---|---|---|
| AuNPs/MWCNTs/GCE | SWV | Myricetin:0.05–40<br>Rutin: — | 12<br>— | [16] |
| Polyfurfural film/GCE | DPV | Myricetin:0.05–10<br>Rutin: 0.001–10 | 10<br>0.025 | [36] |
| β-CD–Au@PTCA–SWCNHs/GCE | DPV | Myricetin:0.01–10<br>Rutin: 0.01–10 | 3.8<br>4.4 | [37] |
| MIP/GO–MWCNTs/GCE | DPV | Myricetin: —<br>Rutin: 0.01–1 | —<br>5 | [56] |
| Cu–CS/MWCNTs/GCE | DPV | Myricetin: —<br>Rutin: 0.05–100 | —<br>10 | [57] |
| PSSA/CNTs/MBT/Au/GCE | DPV | Myricetin: —<br>Rutin: 0.8–10 | —<br>1.8 | [58] |
| Ni-GO/GCE | DPV | Myricetin: —<br>Rutin: 0.011–15 | —<br>3.2 | [59] |
| Pt@r-GO@MWCNTs/GCE | DPV | Myricetin: 0.05–50<br>Rutin: 0.05–50 | 10<br>5 | This work |

current and concentration with linear equations of $I_p$ (μA) = 1.9321C (μM) + 1.9984 ($R^2$ = 0.9901) and $I_p$ (μA) = 0.6533C (μM) + 14.8210 ($R^2$ = 0.9947), respectively. DPVs of the individual quantitative determination of different rutin concentrations in the presence of 2 μM myricetin in the pH 3 BR buffer solution are shown in Fig. 8C. The oxidation peak current and concentration showed two linear detection ranges of 0.05–10 and 10–50 μM (Fig. 8D) with linear equations of $I_p$ (μA) = 2.6258C (μM) + 3.1559 ($R^2$ = 0.9900) and $I_p$ (μA) = 0.6131C (μM) + 22.6930 ($R^2$ = 0.9977), respectively.

The simultaneous quantitative determination of myricetin and rutin at the Pt@r-GO@MWCNTs/GCE was investigated via DPVs. From Fig. 8E, with an increase in concentration of myricetin and rutin, the corresponding oxidation peaks current gradually increased in intensity. Fig. 8F shows that the concentration of myricetin and oxidation peak current exhibited two linear detection ranges of 0.05–10 and 10–50 μM with linear equations of $I_p$ (μA) = 2.0561C (μM) + 1.6368 ($R^2$ = 0.9958) and $I_p$ (μA) = 0.5643C (μM) + 17.2910 ($R^2$ = 0.9731), respectively. From Fig. 8G, the concentration of rutin and oxidation peak current showed two linear detection ranges of 0.05–10 and 10–50 μM with equations of $I_p$ (μA) = 2.4047C (μM) + 3.5326 ($R^2$ = 0.9944) and $I_p$ (μA) = 0.6247C (μM) + 21.6050 ($R^2$ = 0.9906), respectively. The detection limits of myricetin and rutin were 10 and 5 nM (S/N = 3), respectively. These results indicated that the Pt@r-GO@MWCNTs nanocomposite modified electrode showed higher sensitivity and selectivity for both myricetin and rutin. Moreover, compared to other reported determinations of myricetin or rutin, our Pt@r-GO@MWCNTs/GCE can realize the simultaneous determination of myricetin and rutin with lower detection limits and the wider linear ranges (Table 1) [16,36,37,56–59]. The electrode modified with the Pt@r-GO@MWCNTs nanocomposite showed improved detection sensitivity due to the pre-concentration ability and solid-phase extraction.

### 3.8. Reproducibility and stability of the sensor

We also explored the effects of potentially interfering inorganic ions and organic molecules. When 1000-fold excesses of $NaNO_3$, $NH_4F$, $MnSO_4$, $CaCl_2$, and $Zn(AC)_2$, and 100-fold excesses of citric acid, tartaric acid, cystine, glucose, ascorbic acid, and oxalic acid were added, as shown in Table 2, no significant signal changes were observed for oxidation peaks currents of myricetin and rutin, indicating that the assay was not disturbed. These results indicate that the modified electrode exhibited good selectivity for the determination of myricetin and rutin. Furthermore, three modified electrodes were stored under refrigerated conditions (4 °C) and used regularly for myricetin and rutin analysis at 10-day intervals. After 30 days of storage, the sensor response remained quite stable (the reduction of the sensor output signal was ˂5%), demonstrating the excellent stability of Pt@r-GO@MWCNTs/GCE. The reversibility of the Pt@r-GO@MWCNTs/GCE electrode was investigated by DPVs. We modified an electrode that was stored under refrigerated conditions and subsequently used for myricetin and rutin analysis at 8 h intervals for two days. The standard deviation of the oxidation peak currents of the myricetin and rutin was (3.54 ± 0.41) %, indicating good reversibility.

### 3.9. Simultaneous determination of myricetin and rutin in real orange juice samples

The actual analytical application of the prepared Pt@r-GO@MWCNTs/GCE sensor for the simultaneous determination of myricetin and rutin in real orange juice was achieved by standard addition. Three parallel experiments were performed for all measurements. As shown in Table 3, the real orange juice sample recovery rate ranged between 100.57% and 108.46%, and the RSD value was ˂6%. These results indicated that the prepared sensor can be successfully applied for the actual simultaneous determination of myricetin and rutin in real orange juice samples.

## 4. Conclusions

In summary, we successfully manufactured a novel

**Table 2**
Effect of potentially interfering inorganic ions and organic molecules on the oxidation peak current signals of 50 μM myricetin and rutin in the pH 3 BR buffer solution at the Pt@r-GO@MWCNTs/GCE ($n$ = 3).

| Interferences | Concentration (mol/L) | Signal change (%) | |
|---|---|---|---|
| | | Myricetin | Rutin |
| $NaNO_3$ | 0.05 | 4.67 ± 0.91 | 1.07 ± 0.29 |
| $NH_4F$ | 0.05 | −1.53 ± 0.26 | −0.04 ± 0.28 |
| $MgSO_4$ | 0.05 | 1.60 ± 0.29 | −2.09 ± 0.85 |
| $CaCl_2$ | 0.05 | −4.33 ± 0.38 | −2.01 ± 0.92 |
| $Zn(AC)_2$ | 0.05 | 0.78 ± 0.33 | 3.36 ± 0.24 |
| Citric acid | 0.005 | 4.41 ± 0.78 | −3.07 ± 0.36 |
| Tartaric acid | 0.005 | 5.62 ± 0.33 | −3.84 ± 0.66 |
| Cystine | 0.005 | 3.98 ± 0.44 | −2.20 ± 0.35 |
| Glucose | 0.005 | 4.66 ± 0.63 | 3.03 ± 0.50 |
| Ascorbic acid | 0.005 | 5.10 ± 0.24 | 2.03 ± 0.23 |
| Oxalic acid | 0.005 | −4.65 ± 0.35 | −5.17 ± 0.65 |

**Table 3**
Simultaneous determination of myricetin and rutin in real orange juice samples ($n = 3$).

| Sample | Added (μM) | Found[a] (μM) | Recovery (%) | RSD (%) |
|---|---|---|---|---|
| Myricetin | 30 | 32.38 ± 1.26 | 107.92 | 1.6 |
| | 10 | 10.50 ± 0.32 | 105.04 | 1.2 |
| | 0.5 | 0.5423 ± 0.0790 | 108.46 | 5.9 |
| | 0.3 | 0.3017 ± 0.0058 | 100.57 | 0.8 |
| Rutin | 30 | 31.77 ± 1.95 | 105.89 | 2.5 |
| | 10 | 10.11 ± 0.16 | 101.10 | 0.6 |
| | 0.5 | 0.5334 ± 0.0600 | 106.68 | 4.5 |
| | 0.3 | 0.3167 ± 0.0220 | 105.50 | 2.8 |

electrochemical sensor based on a ternary Pt@r-GO@MWCNTs nanocomposite. The nanocomposite sensor exhibited improved detection sensitivity due to the superior pre-concentration ability of the nanocomposite for myricetin and rutin. Under the optimized conditions, the oxidation peak currents of myricetin were proportional to its concentration with linearity ranging from 0.05 to 50 μM and a detection limit of 0.01 μM (S/N = 3). For rutin the linear range was from 0.05 to 50 μM with a detection limit of 0.005 μM (S/N = 3). The sensor also exhibited good reproducibility and stability, and was successfully used for the simultaneous determination of myricetin and rutin in real orange juice samples providing satisfactory results.

## Acknowledgments

This work was financially supported by the National Natural Science Foundation of China (Grant No. 21874047, 21475046, 21427809).

## Conflicts of interest

The authors declare that there are no conflicts of interest.

## References

[1] Z. Liu, A. Zhang, Y. Guo, et al., Electrochemical sensor for ultrasensitive determination of isoquercitrin and baicalin based on DM-beta-cyclodextrin functionalized graphene nanosheets, Biosens. Bioelectron. 58 (2014) 242–248.
[2] Y. Yao, Y. Xie, C. Hong, et al., Development of a myricetin/hydroxypropyl-beta-cyclodextrin inclusion complex: preparation, characterization, and evaluation, Carbohydr. Polym. 110 (2014) 329–337.
[3] K. Zhang, J. Xu, X. Zhu, et al., Poly (3,4-ethylenedioxythiophene) nanorods grown on graphene oxide sheets as electrochemical sensing platform for rutin, J. Electroanal. Chem. 739 (2015) 66–72.
[4] J. Wang, H. Wang, S. Han, Ultrasensitive determination of epicatechin, rutin, and quercetin by capillary electrophoresis chemiluminescence, Acta Chromatogr. 24 (2012) 679–688.
[5] S. Şanli, C. Lunte, Determination of eleven flavonoids in chamomile and linden extracts by capillary electrophoresis, Anal. Meth. 6 (2014) 3858–3864.
[6] D. Yang, H. Li, Z. Hao, et al., Determination of rutin by flow injection chemiluminescence method using the reaction of luminol and potassium hexacyanoferrate(III) with the aid of response surface methodology, Luminescence 25 (2010) 436–444.
[7] A. Kumar, A.K. Malik, D.K. Tewary, A new method for determination of myricetin and quercetin using solid phase microextraction-high performance liquid chromatography-ultra violet/visible system in grapes, vegetables and red wine samples, Anal. Chim. Acta 631 (2009) 177–181.
[8] H. Xu, Y. Li, H.-W. Tang, et al., Determination of rutin with UV-VIS spectrophotometric and laser-induced fluorometric detection using a non-scanning spectrometer, Anal. Lett. 43 (2010) 893–904.
[9] V.K. Gupta, A. Nayak, S. Agarwal, et al., Recent advances on potentiometric membrane sensors for pharmaceutical analysis, Comb. Chem. High. T SCR. 14 (2011) 284–302.
[10] V.K. Gupta, B. Sethi, R.A. Sharma, et al., Mercury selective potentiometric sensor based on low rim functionalized thiacalix [4]-arene as a cationic receptor, J. Mol. Liq. 177 (2013) 114–118.
[11] V.K. Gupta, M.R. Ganjali, P. Norouzi, et al., Electrochemical analysis of some toxic metals by ion-selective electrodes, Crit. Rev. Anal. Chem. 41 (2011) 282–313.
[12] S.K. Srivastava, V.K. Gupta, S. Jain, et al., Determination of lead using a poly(vinyl chloride)-based crown ether membrane, Analyst 120 (1995) 495–498.
[13] S.K. Srivastava, V.K. Gupta, M.K. Dwivedi, et al., Caesium PVC–crown (dibenzo-24-crown-8) based membrane sensor, Anal. Proc. 32 (1995) 21–23.
[14] V.K. Gupta, H. Karimi-Maleh, R. Sadegh, Simultaneous determination of hydroxylamine, phenol and sulfite in water and waste water samples using a voltammetric nanosensor, Int. J. Electrochem. Sci. 10 (2015) 303–316.
[15] S. Komorsky-Lovric, I. Novak, Abrasive stripping voltammetry of myricetin and dihydromyricetin, Electrochim. Acta 98 (2013) 153–156.
[16] R. Hajian, N.A. Yusof, T. Faragi, et al., Fabrication of an electrochemical sensor based on gold nanoparticles/carbon nanotubes as nanocomposite materials: determination of myricetin in same drinks, PLoS One 9 (2014), e96686.
[17] A.K. Jain, V.K. Gupta, L.P. Singh, Neutral carrier and organic resin based membranes as sensors for uranyl ions, Anal. Proc. 32 (1995) 263–266.
[18] A.K. Jain, V.K. Gupta, B.B. Sahoo, et al., Copper(II)-selective electrodes based on macrocyclic compounds, Anal. Proc. 32 (1995) 99–101.
[19] V.K. Gupta, A.K. Singh, L.K. Kumawat, et al., Thiazole Schiff base turn-on fluorescent chemosensor for $Al^{3+}$ ion, Sensor. Actuator. B Chem. 195 (2014) 98–108.
[20] S.K. Srivastava, V.K. Gupta, S. Jain, PVC-based 2,2,2-cryptand sensor for zinc ions, Anal. Chem. 68 (1996) 1272–1275.
[21] B.W. Neuman, G. Kiss, A.H. Kunding, et al., A structural analysis of M protein in coronavirus assembly and morphology, J. Struct. Biol. 174 (2011) 11–22.
[22] V.K. Gupta, S. Kumar, R. Singh, et al., Cadmium (II) ion sensing through p-tert-butyl calix[6]arene based potentiometric sensor, J. Mol. Liq. 195 (2014) 65–68.
[23] Y.-S. Fang, X.-J. Huang, L.-S. Wang, et al., An enhanced sensitive electrochemical immunosensor based on efficient encapsulation of enzyme in silica matrix for the detection of human immunodeficiency virus p24, Biosens. Bioelectron. 64 (2015) 324–332.
[24] T. Zheng, Q. Zhang, S. Feng, et al., Robust nonenzymatic hybrid nanoelectrocatalysts for signal amplification toward ultrasensitive electrochemical cytosensing, J. Am. Chem. Soc. 136 (2014) 2288–2291.
[25] Y.-S. Fang, S.-Y. Chen, X.-J. Huang, et al., Simple approach for ultrasensitive electrochemical immunoassay of Clostridium difficile toxin B detection, Biosens. Bioelectron. 53 (2014) 238–244.
[26] Y. Zhu, P. Chandra, Y.-B. Shim, Ultrasensitive and selective electrochemical diagnosis of breast cancer based on a hydrazine-Au nanoparticle-aptamer bioconjugate, Anal. Chem. 85 (2013) 1058–1064.
[27] Y.-H. Bai, J.-J. Xu, H.-Y. Chen, Selective sensing of cysteine on manganese dioxide nanowires and chitosan modified glassy carbon electrodes, Biosens. Bioelectron. 24 (2009) 2985–2990.
[28] S. Mukdasai, U. Crowley, M. Pravda, et al., Electrodeposition of palladium nanoparticles on porous graphitized carbon monolith modified carbon paste electrode for simultaneous enhanced determination of ascorbic acid and uric acid, Sens. Actuators, B 218 (2015) 280–288.
[29] S. Karthikeyan, V.K. Gupta, R. Boopathy, et al., A new approach for the degradation of high concentration of aromatic amine by heterocatalytic Fenton oxidation: kinetic and spectroscopic studies, J. Mol. Liq. 173 (2012) 153–163.
[30] M.H. Dehghani, D. Sanaei, I. Ali, et al., Removal of chromium(VI) from aqueous solution using treated waste newspaper as a low-cost adsorbent: kinetic modeling and isotherm studies, J. Mol. Liq. 215 (2016) 671–679.
[31] X. Xu, L. Yu, G. Chen, Determination of flavonoids in Portulaca oleracea L. by capillary electrophoresis with electrochemical detection, J. Pharm. Biomed. Anal. 41 (2006) 493–499.
[32] J. Xia, Z. Wang, F. Cai, et al., An electrochemical sensor for the sensitive detection of rutin based on a novel composite of activated silica gel and graphene, RSC Adv. 5 (2015) 39131–39137.
[33] J. Leng, P. Li, L. Bai, et al., Facile synthesis of Pd nanoparticles-graphene oxide hybrid and its application to the electrochemical determination of rutin, Int. J. Electrochem. Sci. 10 (2015) 8522–8530.
[34] Y. Lei, D. Du, L.N. Tang, et al., Determination of rutin by a graphene-modified glassy carbon electrode, Anal. Lett. 48 (2015) 894–906.
[35] S. Yang, G. Li, J. Zhao, et al., Electrochemical preparation of Ag nanoparticles/poly (methylene blue) functionalized graphene nanocomposite film modified electrode for sensitive determination of rutin, J. Electroanal. Chem. 717–718 (2014) 225–230.
[36] J. Huang, X. Shen, Q. Hu, et al., High sensitivity simultaneous determination of myricetin and rutin using a polyfurfuryl film modified glassy carbon electrode, RSC Adv. 6 (2016) 95435–95441.
[37] X. Ran, L. Yang, J. Zhang, et al., Highly sensitive electrochemical sensor based on beta-cyclodextrine-gold@3, 4, 9, 10-perylene tetracarboxylic acid functionalized single-walled carbon nanohorns for simultaneous determination of myricetin and rutin, Anal. Chim. Acta 892 (2015) 85–94.
[38] A. Asfaram, M. Ghaedi, S. Agarwal, et al., Removal of basic dye Auramine-O by ZnS:Cu nanoparticles loaded on activated carbon: optimization of parameters using response surface methodology with central composite design, RSC Adv. 5 (2015) 18438–18450.
[39] V.K. Gupta, N. Atar, M.L. Yola, et al., A novel magnetic Fe@Au core-shell nanoparticles anchored graphene oxide recyclable nanocatalyst for the reduction of nitrophenol compounds, Water Res. 48 (2014) 210–217.
[40] M.L. Yola, V.K. Gupta, T. Eren, et al., A novel electro analytical nanosensor based on graphene oxide/silver nanoparticles for simultaneous determination

of quercetin and morin, Electrochim. Acta 120 (2014) 204–211.
[41] I. Cesarino, V. Cesarino, M.R.V. Lanza, Carbon nanotubes modified with antimony nanoparticles in a paraffin composite electrode: simultaneous determination of sulfamethoxazole and trimethoprim, Sens. Actuators, B 188 (2013) 1293–1299.
[42] K. Gong, X. Wu, G. Zhao, et al., Tribological properties of polymeric aryl phosphates grafted onto multi-walled carbon nanotubes as high-performances lubricant additive, Tribol. Int. 116 (2017) 172–179.
[43] D.A.C. Brownson, C.E. Banks, Graphene electrochemistry: an overview of potential applications, Analyst 135 (2010) 2768–2778.
[44] S. Palanisamy, V. Velusamy, S.-W. Chen, et al., Enhanced reversible redox activity of hemin on cellulose microfiber integrated reduced graphene oxide for $H_2O_2$ biosensor applications, Carbohydr. Polym. 204 (2019) 152–160.
[45] W. Chen, S. Cai, Q.-Q. Ren, et al., Recent advances in electrochemical sensing for hydrogen peroxide: a review, Analyst 137 (2012) 49–58.
[46] A.G. Nandgaonkar, Q. Wang, K. Fu, et al., A one-pot biosynthesis of reduced graphene oxide (RGO)/bacterial cellulose (BC) nanocomposites, Green Chem. 16 (2014) 3195–3201.
[47] C. Lee, X. Wei, J.W. Kysar, et al., Measurement of the elastic properties and intrinsic strength of monolayer graphene, Science 321 (2008) 385–388.
[48] V.K. Gupta, N. Mergu, L.K. Kumawat, et al., Selective naked-eye detection of Magnesium (II) ions using a coumarin-derived fluorescent probe, Sens. Actuators, B 207 (2015) 216–223.
[49] V.K. Gupta, N. Mergu, L.K. Kumawat, et al., A reversible fluorescence "off-on-off" sensor for sequential detection of aluminum and acetate/fluoride ions, Talanta 144 (2015) 80–89.
[50] H. Karimi-Maleh, F. Tahernejad-Javazmi, N. Atar, et al., A novel DNA biosensor based on a pencil graphite electrode modified with polypyrrole/functionalized multiwalled carbon nanotubes for determination of 6-mercaptopurine anticancer drug, Ind. Eng. Chem. Res. 54 (2015) 3634–3639.
[51] F.C. Moraes, M.F. Cabral, L.H. Mascaro, et al., The electrochemical effect of acid functionalization of carbon nanotubes to be used in sensors development, Surf. Sci. 605 (2011) 435–440.
[52] M.L. Yola, T. Eren, N. Atar, et al., Direct-methanol fuel cell based on functionalized graphene oxide with mono-metallic and bi-metallic nanoparticles: electrochemical performances of nanomaterials for methanol oxidation, Electroanalysis 28 (2016) 570–579.
[53] V. Georgakilas, D. Gournis, V. Tzitzios, et al., Decorating carbon nanotubes with metal or semiconductor nanoparticles, J. Mater. Chem. 17 (2007) 2679–2694.
[54] H. Yang, Q. Shi, Y. Song, et al., Glucose biosensor based on mesoporous Pt nanotubes, J. Electrochem. Soc. 164 (2017) B230–B233.
[55] M.L. Yola, N. Atar, Functionalized graphene quantum dots with bi-metallic nanoparticles composite: sensor application for simultaneous determination of ascorbic acid, dopamine, uric acid and tryptophan, J. Electrochem. Soc. 163 (2016) B718–B725.
[56] L. Yang, J. Yang, B. Xu, et al., Facile preparation of molecularly imprinted polypyrrole-graphene-multiwalled carbon nanotubes composite film modified electrode for rutin sensing, Talanta 161 (2016) 413–418.
[57] M.B. Gholivand, L. Mohammadi-Behzad, H. Hosseinkhani, Application of a Cu-chitosan/multiwalled carbon nanotube film-modified electrode for the sensitive determination of rutin, Anal. Biochem. 493 (2016) 35–43.
[58] M. Arvand, M. Farahpour, M.S. Ardaki, Electrochemical characterization of in situ functionalized gold organosulfur self-assembled monolayer with conducting polymer and carbon nanotubes for determination of rutin, Talanta 176 (2018) 92–101.
[59] S.U. Karabiberoglu, Z. Dursun, Fabrication of nickel coated graphene oxide composite electrode for sensitive determination of rutin, J. Electroanal. Chem. 815 (2018) 76–85.